Energy and system size dependence of chemical freeze-out in relativistic nuclear collisions.

F. Becattini
Università di Firenze and INFN Sezione di Firenze, Florence, Italy

J. Manninen
University of Oulu, Oulu, Finland

M. Gaździcki
Institut für Kernphysik, Universität Frankfurt, Frankfurt, Germany and Świętokrzyska Academy, Kielce, Poland

We present a detailed study of chemical freeze-out in p-p, C-C, Si-Si and Pb-Pb collisions at beam momenta of 158A GeV as well as Pb-Pb collisions at beam momenta of 20A, 30A, 40A and 80A GeV. By analyzing hadronic multiplicities within the statistical hadronization model, we have studied the parameters of the source as a function of the number of the participating nucleons and the beam energy. We observe a nice smooth behaviour of temperature, baryon chemical potential and strangeness under-saturation parameter as a function of energy and nucleus size. Interpolating formulas are provided which allow to predict the chemical freeze-out parameters in central collisions at centre-of-mass energies $\sqrt{s}_{NN} \gtrsim 4.5$ GeV and for any colliding ions. Specific discrepancies between data and model emerge in particle ratios in Pb-Pb collisions at SPS between 20A and 40A GeV of beam energy which cannot be accounted for in the considered model schemes.

I. INTRODUCTION

The main goal of the ultra-relativistic nucleus-nucleus (AA) collisions programme is to create in terrestrial laboratories a new state of matter, the Quark-Gluon Plasma (QGP). The existence of this phase, where quarks and gluons are deconfined, i.e. can freely move over several hadronic distances, is a definite prediction of Quantum Chromo-Dynamics (QCD). In the search for QGP, signals in nucleus-nucleus collisions at different nucleon-nucleon centre of mass ($\sqrt{s}_{NN}$) energies have been studied: from few GeV at AGS to several hundreds of GeV recently attained in Au-Au collisions at RHIC.

One of the main results is the surprising success of the statistical-thermal models in reproducing essential features of particle production [1]. This model succeeds also in describing particle multiplicities in many kinds of elementary collisions [2], suggesting that statistical production is a general property of the hadronization process itself [2, 3]. Furthermore, the statistical hadronization model (SHM) supplemented with the hydrodynamical expansion of the matter, to a large extent, also reproduces transverse momentum spectra of different particle species [4].

Hence, the SHM model proves to be a useful tool for the analysis of soft hadron production and particularly to study strangeness production, whose enhancement has since long been proposed as a signature of QGP formation. Furthermore, anomalies in the energy dependence of strangeness production have been predicted [5] as a signature of deconfinement and have been indeed observed experimentally [6].

In a recent paper of ours [7], we have studied these topics in detail comparing different versions of the statistical model. More recently, new experimental results [8] of hadronic multiplicities at top SPS beam energy - i.e. 158 A GeV, corresponding to $\sqrt{s}_{NN} = 17.2$ GeV - with light ion collisions (C-C and Si-Si), as well as in Pb-Pb collisions at beam energies of 20 and 30 A GeV- corresponding to $\sqrt{s}_{NN} = 6.2$ and 7.5 GeV respectively - became available. The Pb-Pb data has been recently analyzed [9] within a version of the statistical model including a light-quark non-equilibrium parameter, γ_q. In the present work, we study the energy and system size dependence of chemical freeze-out by performing a systematic analysis of the available data within a more essential framework of the SHM, including only the strangeness under-saturation parameter γ_S. With the updated data sample, we also test a two-component version of the SHM, where particle production stems from the superposition of fully chemically equilibrated fireballs and single nucleon-nucleon collisions; we also briefly address, once again, the issue whether the non-equilibrium factor γ_q is allowed.

The paper is organized as follows: a brief discussion on the SHM is given in Sect. 2. In Sect. 3 the experimental data selected for the analysis and the results of the analysis in our main and alternative schemes of the SHM are given. In Sect. 4 we present and discuss the energy and system size dependence of the chemical freeze-out stage. A general discussion of our results and the observed deviations from the data is given in Sect. 5. Conclusions are drawn in Sect. 6.

II. THE STATISTICAL HADRONIZATION MODEL IN HEAVY ION COLLISIONS

The statistical hadronization model has been described in detail elsewhere [7]. Here we briefly summarize its founding concepts and discuss the issue of full-phase-space versus midrapidity analysis.

The main idea of the statistical hadronization model is that hadrons are formed in statistical equilibrium within extended excited regions called *fireballs* or *clusters*. Several fireballs or clusters are produced in a single collision as a result of a dynamical process, each having a definite total momentum, charges and volume.

In principle, the overall particle multiplicity should be calculated by adding those relevant to single clusters and folding with the probability distribution of volumes, masses (being Lorentz invariants, they are independent of clusters' momenta) and charges. Unfortunately this calculation is not possible within the SHM alone, because fluctuations of volumes, charges and masses of clusters, being governed by the previous dynamical process, are not known. However, if they happen to be the same as those relevant to the random partitioning of one large cluster - defined as *equivalent global cluster* (EGC) - having as volume the sum of all clusters' rest frame volumes - the overall particle multiplicities turn out to be simply those the EGC [7], which has charges equal to the sum of single clusters' charges in compliance of conservation laws. The straightforward consequence of such an assumption is that, in order to calculate full phase space mean multiplicities, one can use a simple single-cluster (i.e. the EGC) formula. Of course, this is just a phenomenological simplifying assumption and it should *not* be expected to be fully true; deviations from this simple picture should show up as second-order deviations between data and model.

It is very important to emphasize that the EGC picture takes advantage of the independence of particle multiplicity (as well as any other Lorentz scalar) on clusters' momenta and, consequently, on any dynamical charge-momentum correlation. This means that the hypothesis of single EGC calculation may hold even if clusters with large baryon number (and density) are likely to have large rapidity.

To show this in simplest terms, let us consider events with N clusters and let $w(Q_1, y_1; \ldots; Q_N, y_N)$ the probability of having the i^{th} cluster with charge Q_i at rapidity y_i. The overall average particle multiplicity of the species j reads:

$$\langle\langle n_j\rangle\rangle = \sum_{Q_1,\ldots,Q_N} \int \mathrm{d}y_1 \ldots \mathrm{d}y_N \; w(Q_1, y_1; \ldots; Q_N, y_N) \langle n_j\rangle(Q_1, y_1; \ldots; Q_N, y_N), \tag{1}$$

where $\langle n_j\rangle(Q_1, y_1; \ldots; Q_N, y_N)$ is the average multiplicity of the species j for a particular charge and rapidity configuration. Now, being a Lorentz scalar, $\langle n_j\rangle$ can only depends on charges, hence in fact $\langle n_j\rangle = \langle n_j\rangle(Q_1, \ldots, Q_N)$. Therefore:

$$\langle\langle n_j\rangle\rangle = \sum_{Q_1,\ldots,Q_N} W(Q_1, \ldots, Q_N) \langle n_j\rangle(Q_1, \ldots, Q_N) \tag{2}$$

where:

$$W(Q_1, \ldots, Q_N) = \int \mathrm{d}y_1 \ldots \mathrm{d}y_N \; w(Q_1, y_1; \ldots; Q_N, y_N).$$

Thus, in order to reduce to the simple EGC case, we have to introduce some hypothesis on the form of the *marginal* distribution of charges $W(Q_1, \ldots, Q_N)$ in Eq. (2) and we do not need to deal anymore with the full distribution of charges and rapidities w in Eq. (1); charge-rapidity correlations have disappeared.

In a different approach, used in several works, the formulas of the statistical model are assumed to apply only to the *average* (with respect to all kinds of fluctuations) fireball at midrapidity. The charge probability distribution $\omega(Q, y)$ of a fireball at rapidity y is obtained from the general w in Eq. (1) by integrating over all rapidities:

$$\omega(Q, y) \propto \sum_{i=1}^{N} \sum_{Q_1,\ldots,Q_N} \delta_{Q,Q_i} \int \mathrm{d}y_1 \ldots \mathrm{d}y_N \; w(Q_1, y_1; \ldots; Q_N, y_N) \delta(y - y_i) \tag{3}$$

Thus, in order to perform a statistical model fit, one would need to assume only that charge fluctuations at midrapidity, i.e. $\omega(Q, 0)$, are not too large, which is apparently a less restrictive requirement than that needed to ensure the validity of the EGC approach. In order to estimate the parameters of the average central fireball, the idea is then to use particle yields and ratios measured at midrapidity rather than in full phase space. However, these yields do not single out the production from the central fireball as also nearby clusters contribute to them and, if they have quite different mean charges, one would not get the desired result. Moreover, if a single cluster was formed at rest in the centre-of-mass frame, a cut on a midrapidity window ($\Delta y \approx 1$) would introduce a bias in the estimation of thermal parameters because rapidity distributions are narrower for more massive particles (see e.g. discussion in ref. [7]). The

general effect would be an increase in the fitted temperature and strangeness under-saturation parameter γ_S, what is indeed the case in an analysis at SPS using midrapidity densities [10]. In fact, narrower rapidity distributions for more massive particles have been measured up to top SPS energy ($\sqrt{s}_{NN} \sim 20$ GeV). For this approach to yield consistent results, one would need a distribution of clusters with an approximately uniform charge and energy densities over a sufficiently large rapidity region, i.e. larger than the typical width of single cluster's particle rapidity spectrum. To show this, we start by writing the rapidity spectrum of a particle as:

$$\frac{\mathrm{d}N}{\mathrm{d}y} = \int_{-\infty}^{+\infty} \mathrm{d}Y \; \rho(Y) \, \frac{\mathrm{d}n}{\mathrm{d}y} \left(\mu(Y), T(Y), y - Y\right) \tag{4}$$

where $\rho(Y)$ is the density of clusters at rapidity Y and $\mathrm{d}n/\mathrm{d}y$ is the primordial rapidity spectrum of particles emitted from the cluster with rapidity Y. Changing the integration variable to $y' = y - Y$, one obtains:

$$\frac{\mathrm{d}N}{\mathrm{d}y} = \int_{-\infty}^{+\infty} \mathrm{d}y' \; \rho(y - y') \, \frac{\mathrm{d}n}{\mathrm{d}y} \left(\mu(y - y'), T(y - y'), y'\right). \tag{5}$$

If $\rho(y - y')$ is approximately constant over a rapidity range (around y) sufficiently larger than the width of $\mathrm{d}n/\mathrm{d}y$, and so are $T(y - y')$ and $\mu(y - y')$, then:

$$\frac{\mathrm{d}N}{\mathrm{d}y} \approx \rho(y) \int_{-\infty}^{+\infty} \mathrm{d}y' \; \frac{\mathrm{d}n}{\mathrm{d}y} \left(\mu(y), T(y), y'\right) = \rho(y) \, n(T(y), \mu(y)) \tag{6}$$

hence the rapidity density turns out to be proportional to the number of particles emitted from the average cluster at rapidity y. This condition also implies that the measured $\mathrm{d}N/\mathrm{d}y$ is approximately constant over the same range.

However, this necessary condition is not met at centre-of-mass energies $\sqrt{s}_{NN}$ up to $20A$ GeV, as measured rapidity distributions have a width not much larger than those from a single cluster at the kinetic freeze out. For instance, for pions at top SPS energy, the expected dispersion of the central cluster's rapidity distribution at a kinetic freeze-out temperature of $T \approx 125$ MeV, is about 0.8 while the dispersion of the actual distribution is $\simeq 1.3$ [11]. On the other hand, the measured width at $\sqrt{s}_{NN} = 200$ at RHIC is ≈ 2 for pions [12] and antiparticle/particle ratio is apparently stable over a rapidity window of about 2 units around midrapidity [13]. These two observations indicate that extracting the characteristics of the average source at midrapidity by using midrapidity ratios is indeed possible at centre-of-mass energies $\mathcal{O}(100)$ GeV. Then, we conclude that the use of full phase space multiplicities is better suited over the energy range of AGS and SPS, that we are examining in the present work, whilst midrapidity particle ratios can be used at RHIC energies to determine the characteristics of the central source. Even though a statistical model fit to full phase space multiplicities at RHIC in principle may be attempted, provided that the EGC condition applies, the presently available data set is not sufficient to make a reliable assessment.

III. THE DATA ANALYSIS

The experimental data set consists of measurements performed by NA49 collaboration in p-p (all inelastic reactions), C-C (15.3% most central), Si-Si (12.2% most central) collisions at beam momentum of $158A$ GeV as well as Pb-Pb collisions at beam momenta of $20A$, $30A$, $40A$, $80A$ and $158A$ GeV (corresponding to $\sqrt{s}_{NN} = 6.2$, 7.5, 8.7, 12.3 and 17.2 GeV, respectively). The Pb-Pb data set corresponds to 7% most central events except at top energy, where only 5% thereof was selected. We also refit measurements in Au-Au collisions at $11.6A$ GeV of beam momentum (corresponding to $\sqrt{s}_{NN} = 4.7$ GeV) by using the new hadronic data set input [14].

The analysis is performed by searching the minima of the χ^2:

$$\chi^2 = \sum_i \frac{(N_i^{\mathrm{exp}} - N_i^{\mathrm{theo}})^2}{\sigma_i^2} \tag{7}$$

in which N_i is the full phase space of the i^{th} hadron species and $\sigma_i = \sqrt{(\sigma_i^{syst})^2 + (\sigma_i^{stat})^2}$ is the sum in quadrature of statistical and systematic experimental error.

The theoretical multiplicities are calculated by adding the primary multiplicities to the contribution from secondary decays. In order to make a proper comparison with the data, the decay chain is stopped so as to match the experimental definition of measured particle. For SPS data, weakly decaying particles are considered as stable, except Λ and $\bar{\Lambda}$ at $20A$ and $30A$ GeV, whereas for AGS Au-Au collisions, weak decays of hyperons and K^0_S are performed. The final experimental and theoretical multiplicities used in our analysis are shown in Tables III, IV and V.

We have performed the analysis with two independent programs, hereafter referred to as analyses A and B, to cross check the results and to assess the stability of the fits. We find only small discrepancies between the different analyses, mainly owing to a different method of treating hidden strangeness, branching ratios and a slightly different particle input. The effect of uncertainties in masses, widths and branching ratios have been shown to be negligible [7] and the difference in results between the two analyses arises solely from the different selection of the included hadronic states. The observed differences in the fit parameters between A and B are of the order of the fit errors and they may be considered as an estimate of the systematic error due to uncertainties in the implementation of the model.

We give two different errors for the fitted parameters and derived quantities in Table I, the first being the error coming out from the fitting program (inferred from the analysis of the $\chi^2 = \chi^2_{\rm min} + 1$ level contours) while the second one is the error rescaled by a factor $\sqrt{\chi^2_{\rm min}/dof}$ where dof is the number of degrees of freedom. We deem that the latter is a more realistic uncertainty on the parameters because of the "imperfect" $\chi^2_{\rm min}/dof$ values (for further details, see [7, 14]), and thus the rescaled errors are used in all plots in this paper.

A. Main version

In our main version of the model we fit the parameters T, V, μ_B and the strangeness under-saturation parameter γ_S; for the relevant formulas, see ref. [7]. This version of the model is called SHM(γ_S). The resulting SHM(γ_S) -parameters (see Table I and Figs. 1, 2, 3 and 4) are smoothly varying functions of the beam energy and no signs of anomalies are present. The fits have been performed in the supposedly sufficient statistical ensemble, i.e canonical (exact conservation of strangeness, electric charge and baryon number) for p-p collisions, S-canonical (exact conservation of strangeness, but with grand-canonical treatment of electric charge and baryon number) in C-C and Si-Si collisions and grand-canonical (GC) for Pb-Pb collisions.

Indeed, for C-C collisions, where the number of participants is quite small, we have cross-checked our main S-canonical calculation with a full canonical calculation in which the baryon number has been set to the nearest integer number to the measured average number of participants. Very little deviations have been found between the two schemes for all particles, thus confirming the fitness of S-canonical ensemble. On the other hand, the grand-canonical ensemble is not well suited both for C-C and Si-Si collisions. By using the best fit parameters in the two pictures and comparing the fitted yields we have found that, for these systems, GC ensemble overestimates the yield of multiply strange hyperons like Ω^- by 32% and 14% respectively with respect to S-canonical ensemble. This clearly indicates that S-canonical scheme is necessary.

The quality of the fits can be regarded as satisfactory overall, although not really good from a statistical point of view (except in Au-Au and C-C collisions) as χ^2/dof's are generally of the order of 2-3. The worst fits are in Pb-Pb collisions at 20A and 30A GeV, with $\chi^2/dof \sim 3-4$; this owes to specific deviations involving strange particles, that will be discussed in detail later in Sect. 5.

A special mention is needed for p-p collisions. As has been mentioned, theoretical multiplicities have been calculated in the canonical ensemble, which is described in detail in ref. [15]. As far as strangeness under-saturation is concerned, in the analysis B, the usual parametrization with γ_S has been used. On the other hand, in the analysis A, a parametrization described in ref. [15] has been used in which it is assumed that some number of ßpairs, poissonianly distributed, hadronizes. The parameter γ_S is thus replaced by the mean number $\langle s\bar{s}\rangle$ of these ßpairs. In general, for p-p, it was not possible to achieve a satisfactory fit in both models. We believe that this owes to the inadequacy of the canonical ensemble at this relatively low energy, where micro-canonical effects play a non- negligible role [16]. For analysis A, a good fit has been obtained removing the ϕ meson from the data sample, whose predicted yield deviates from the data around 70%; indeed, the inclusion of ϕ leads the fit towards exceedingly high temperatures. For analysis B, a fair fit has been obtained removing the Ξ's and Ω's baryons from the data sample. Also in this case, the discrepancy between central data value and model are considerable, but it should be also noted that the likely micro-canonical effects are the largest for heavy baryons in pp collisions [16]. In general, it seems that the parametrization with $\langle s\bar{s}\rangle$ leads to a better agreement with the data in comparison with the γ_S parametrization, according to a cross-test performed in the framework of the analysis A.

B. Proper volume

We have amended our fits by implementing extended hadrons instead of point-like particles. Our calculations follow the model in ref. [17], with a primary average multiplicity of the species j in the grand-canonical ensemble reading,

TABLE I: Summary of fitted parameters in nuclear collisions at AGS and SPS energies in the framework of the SHM(γ_S) model. Also quoted strangeness chemical potential, minimum χ^2's, the estimated radius of the EGC and the λ_S parameter (see Sect. 3). The re-scaled errors, (see text) are quoted within brackets. For p-p at 158A GeV of beam energy, we have fitted mean number of $s\bar{s}$ pairs (analysis A), and fitted γ_S (analysis B).

Parameters	Main analysis A	Main analysis B	Main analysis A	Main analysis B
	p-p 158A GeV (C ensemble)		Au-Au 11.6A GeV (GC ensemble)	
T [MeV]	181.5±3.4[a]	178.2±4.8 (5.9)	118.7±2.7 (3.1)	119.2±3.9 (5.3)
μ_B [MeV]			554.4±11.3 (13.0)	578.8±15.4 (20.9)
γ_S	0.461±0.020[a,b]	0.446±0.018 (0.023)	0.640±0.060 (0.069)	0.768±0.086 (0.116)
VT^3 exp[$-0.7\,\mathrm{GeV}/T$]	6.2±0.5[a,c]	0.127±0.005 (0.006)	1.99±0.17 (0.20)	1.47 ±0.18 (0.25)
χ^2/dof	8.4/10[a]	10.8/7	4.0/3	5.5/3
R [fm]		1.28±0.08 (0.10)	9.25±0.60 (0.69)	8.28±0.71 (0.96)
λ_S	0.266±0.019	0.195±0.005 (0.006)	0.380±0.050 (0.058)	0.489±0.083 (0.11)
	C-C 158A GeV (S-canonical ensemble)		Si-Si 158A GeV (S-canonical ensemble)	
T [MeV]	166.0±4.4 (4.4)	166.1±4.2	162.2±4.9 (7.9)	163.3±3.0 (4.1)
μ_B [MeV]	262.6±12.8 (12.9)	249.0±12.6	260.0±11.1 (17.9)	246.4±11.0 (15.1)
γ_S	0.547±0.041 (0.041)	0.578±0.043	0.621±0.047 (0.076)	0.668±0.049 (0.067)
VT^3 exp[$-0.7\,\mathrm{GeV}/T$]	0.89±0.06 (0.06)	0.83±0.05	2.22±0.14 (0.22)	2.07±0.13 (0.18)
χ^2/dof	4.1/4	3.4/4	10.4/4	7.6/4
R [fm]	2.89±0.19 (0.19)	2.82±0.19	4.15±0.30 (0.48)	3.99±0.19 (0.27)
λ_S	0.373±0.031 (0.032)	0.364±0.034	0.414±0.033 (0.054)	0.418±0.036 (0.049)
	Pb-Pb 20A GeV (GC ensemble)		Pb-Pb 30A GeV (GC ensemble)	
T [MeV]	131.3±2.3 (4.5)	135.8±3.2 (5.2)	140.1±1.6 (3.3)	144.3±1.9 (4.7)
μ_B [MeV]	466.7±6.5 (12.9)	472.5±8.6 (13.7)	413.7±8.0 (16.3)	406.0±8.0 (19.1)
γ_S	0.773±0.037 (0.072)	0.885±0.053 (0.086)	0.773±0.041 (0.084)	0.798±0.040 (0.099)
VT^3 exp[$-0.7\,\mathrm{GeV}/T$]	4.41±0.23 (0.45)	3.88±0.26 (0.42)	6.91±0.40 (0.80)	6.52±0.35 (0.84)
μ_S [MeV]	101.2	114.2	93.2	99.8
χ^2/dof	15.5/4	10.3/4	16.5/4	23.0/4
R [fm]	9.05±0.41 (0.80)	7.89±0.46 (0.73)	8.80±0.32 (0.64)	7.99±0.33 (0.79)
λ_S	0.477±0.035 (0.069)	0.586±0.056 (0.089)	0.500±0.037 (0.073)	0.517±0.039 (0.093)
	Pb-Pb 40A GeV (GC ensemble)		Pb-Pb 80A GeV (GC ensemble)	
T [MeV]	146.1±2.2 (3.0)	143.0±2.3 (3.1)	153.5±2.5 (4.1)	149.9±3.2 (5.1)
μ_B [MeV]	382.4±6.8 (9.1)	380.8±6.6 (8.9)	298.2±5.9 (9.6)	293.8±6.9 (11.0)
γ_S	0.779±0.033 (0.045)	0.857±0.037 (0.050)	0.740±0.024 (0.040)	0.797±0.031 (0.049)
VT^3 exp[$-0.7\,\mathrm{GeV}/T$]	8.75±0.40 (0.54)	7.57±0.35 (0.48)	15.25±0.61 (0.99)	13.53±0.64 (1.03)
μ_S [MeV]	89.5	89.5	69.6	68.4
χ^2/dof	10.9/6	11.0/6	10.6/4	10.2/4
R [fm]	8.53±0.35 (0.47)	8.59±0.35 (0.48)	9.05±0.38 (0.62)	9.23±0.44 (0.70)
λ_S	0.523±0.032 (0.043)	0.513±0.031 (0.042)	0.474±0.023 (0.038)	0.443±0.021 (0.034)
	Pb-Pb 158A GeV (GC ensemble)			
T [MeV]	157.5±1.6 (2.5)	154.6±1.5 (2.7)		
μ_B [MeV]	248.9±5.7 (9.0)	245.9±5.6 (10.0)		
γ_S	0.842±0.027 (0.042)	0.941±0.030 (0.054)		
VT^3 exp[$-0.7\,\mathrm{GeV}/T$]	20.91±0.87 (1.39)	18.21±0.75 (1.35)		
μ_S [MeV]	59.3	59.5		
χ^2/dof	22.5/9	29.1/9		
R [fm]	9.42±0.27 (0.44)	9.42±0.27 (0.48)		
λ_S	0.526±0.020 (0.032)	0.508±0.020 (0.036)		

a - In the fit A, the ϕ meson has been excluded from the data sample because it biased the fit towards an exceedingly high temperature. The final χ^2 does not then take into account the large deviation of ϕ meson yield.

b - In the fit A, the γ_S parameter is to be replaced by the mean number $\langle s\bar{s}\rangle$ of strange quark pairs.

c - In the fit A, the parameter VT^3 exp[$-0.7\,\mathrm{GeV}/T$] is to be replaced by VT^3.

in the limit of Boltzmann statistics:

$$\langle n_j \rangle = \frac{\langle n_j \rangle_{\rm pl} {\rm e}^{-v_j \xi}}{1 + \sum_k (v_k/V) \langle n_k \rangle_{\rm pl} {\rm e}^{-v_k \xi}} \tag{8}$$

where $\langle n_j \rangle_{\rm pl}$ is the hadron multiplicity in the point-like case, ξ is the solution of the equation:

$$\xi = \sum_k \langle n_k \rangle_{\rm pl} {\rm e}^{-v_k \xi} \tag{9}$$

and v_j is the proper volume, or eigenvolume, of the hadron. This volume effectively introduces a repulsive hard-core interaction in the hadron gas equation of state, yet it is an unknown quantity and one has to make some assumptions to develop calculations. If it was the same for all hadrons, there would be no corrections to the intensive parameters, as the ratio between different species would be the same (this can be seen from Eq. 8). We have tested the assumption of an eigenvolume v_j proportional to the mass through a bag-like constant B. In this case, one expects an upward shift in the temperature $\Delta T \simeq T^2 B \xi$, since, for masses $m \gg T$ one has:

$$\langle n_j \rangle \propto \left(\frac{mT}{2\pi} \right)^{3/2} {\rm e}^{-m_j/T - B\xi m_j} \tag{10}$$

with all other fit parameters almost unchanged. Indeed, we have found that, for several reasonable values of the constant B, from 0.5 to 2 fm^3/GeV, the only effect in the fit was a temperature raise by the expected amount without any decrease in the χ^2, that is in the fit quality. We therefore conclude that the introduction of this effect, at least in the model of ref. [17], does not entail an improvement of the agreement data-model with respect to the point-like picture.

TABLE II: Fit results in central C-C, Si-Si and Pb-Pb collisions at 158A GeV within the two-component model SHM(TC) and with $\langle N_c \rangle$ as free parameter (top section) as well as with $\langle N_c \rangle$ fixed to the value calculated in the Glauber model (bottom section). The re-scaled errors (see text) are quoted within brackets.

Parameters	C-C, canonical ensemble	Si-Si, S-canonical ensemble	Pb-Pb, GC ensemble
T [MeV]	172.4±11.8 (12.6)	162.0±7.6	153.9±1.5 (2.5)
μ_B [MeV]		234.4±22.5	240.8±6.9 (11.8)
γ_S	1.0 (fixed)	1.0 (fixed)	1.0 (fixed)
VT^3 exp$[-0.7\,{\rm GeV}/T]$	0.23±0.034 (0.037)	0.91±0.11	16.11±0.57 (0.97)
$\langle N_c \rangle$	6.0±0.4 (0.4)	11.4±1.8	25±10 (16)
χ^2/dof	5.8/4	1.0/4	26.3/9
Parameters	C-C, S-canonical ensemble	Si-Si, S-canonical ensemble	Pb-Pb, GC ensemble
T [MeV]	161.0±9.1 (25.9)	151.1±7.1 (16.4)	154.7±1.5 (2.9)
μ_B [MeV]	315±18 (50)	285±13 (31)	261.6±2.6 (4.6)
γ_S	1.0 (fixed)	1.0 (fixed)	1.0 (fixed)
VT^3 exp$[-0.7\,{\rm GeV}/T]$	0.31±0.028 (0.071)	1.19±0.06 (0.12)	16.54±0.44 (0.84)
$\langle N_c \rangle$	2.67 (fixed)	5.49 (fixed)	17.6 (fixed)
χ^2/dof	32/5	21.7/5	36.3/10

C. Two-component model

In this picture, henceforth referred to as SHM(TC), the observed hadron production is assumed to stem from the superposition of two components (TC): one originated from one or more fireballs in full chemical equilibrium and another component from peripheral single nucleon-nucleon collisions where final particles escape interaction region. The idea of this model is to ascribe the observed under-saturation of strangeness in heavy ion collisions to the N-N component, leaving the large fireballs at complete equilibrium, i.e. with $\gamma_S = 1$. Of course, this is possible provided

that the mean number of single nucleon-nucleon collisions ($\langle N_c \rangle$) is sufficiently large. We note that similar approaches have been proposed in literature where the role of the second component beside the main fireball is played by smaller peripheral fireball with different thermodynamical parameters or by a collection of clusters [18]. It should be mentioned that the SHM(TC) picture is quite a simplified one: it is assumed that particles emerging from N-N collisions decouple without further re-interaction, whereas collisions in the core of the system eventually lead to a hadron gas in perfect equilibrium. These are sharp approximations that would certainly need a refinement in more accurate studies.

In the SHM(TC) model, the overall hadron multiplicity can be written then as:

$$\langle n_j \rangle = \langle N_c \rangle \langle n_j \rangle_{NN} + \langle n_j \rangle_V \tag{11}$$

where $\langle n_j \rangle_{NN}$ is the average multiplicity of the j^{th} hadron in a single N-N collision and $\langle n_j \rangle_V$ is the average multiplicity of hadrons emitted from the equilibrated fireball with $\gamma_S = 1$. The $\langle n_j \rangle_{NN}$ term can be written in turn as:

$$\langle n_j \rangle_{NN} = \frac{Z^2}{A^2} \langle n_j \rangle_{pp} + \frac{(A-Z)^2}{A^2} \langle n_j \rangle_{nn} + \frac{2Z(A-Z)}{A^2} \langle n_j \rangle_{np} \tag{12}$$

To calculate $\langle n_j \rangle_{NN}$ we have used the statistical model and fitted p-p full phase space multiplicities measured at the same beam energy by the same NA49 experiment (see Table III). For n-p and n-n collisions, the parameters of the statistical model determined in p-p are retained and the initial quantum numbers are changed accordingly.

We have fitted T, V, μ_B of the equilibrated fireballs and $\langle N_c \rangle$ by using NA49 data in C-C, Si-Si and Pb-Pb collisions at 158A GeV in the analysis A. It should be mentioned that, in this fit, the systematic error on the refitted parameters owing to the uncertainty on statistical model parameters in N-N collisions (i.e. the errors quoted in Table I for p-p collisions), used as input, has been disregarded. The resulting fit parameters are shown in Table II. For the Pb-Pb system, the fit quality, as well as the obtained values of T and μ_B, are comparable to the main fit within the SHM(γ_S) model. The predicted number of "single" N-N collisions is about 25. Thus, on average, only 310 nucleons out of 360 participants contribute to the formation of large equilibrated fireballs. In case of Si-Si, the fit quality is significantly improved compared to the main version of the statistical model, and the resulting fit parameters are comparable to the ones in Table II. The number of independent N-N collisions is 12±4, suggesting that more than half of the 41 participating nucleons are colliding only once.

Being so small, C-C system needs special treatment when two component model is applied. Since there are only 16 participants in the system, one has to calculate both components in full canonical ensemble. This means that one has to take explicitly into account all different proton-neutron configurations in the central fireball and extract those nucleons participating to the fireball from the 'nucleon pool' available for the single N-N collisions. It seems that even C-C can be described with the two component model if the baryon charge in the central fireball is of the order B=n+p=4. The resulting $\chi^2/dof \simeq 5.8/4$ with all the different n+p=4 combinations in the completely equilibrated fireball, i.e. the fit quality is worse than with the main version of the statistical model, but the overall fit quality is acceptable anyhow.

To cross-check these results, we have calculated the number of single N-N collisions from the Glauber model and repeated the fits (in the analysis B) the same way by fixing $\langle N_c \rangle$ as that coming from the Glauber calculations. We first implemented a Monte-Carlo calculation of the Glauber model as follows:

1. at a given impact parameter, the number of collisions of each projectile nucleon is randomly extracted from a Poisson distribution whose mean is the product of the thickness function times the inelastic nucleon-nucleon cross-section;

2. then, the number of collisions undergone by each nucleon belonging to the target nucleus is randomly extracted from a multinomial distribution constrained with the total number of collisions as determined in the previous step and whose weights are proportional to the product of their relevant thickness function times the inelastic nucleon-nucleon cross-section;

3. for each generated event, uniformly distributed in the transverse impact parameter plane, we keep track of the number of nucleons undergoing $0, 1, 2, \ldots$ collisions $N_0, N_1, N_2, \ldots$ in both projectile and target nucleus.

The thickness function has been calculated on the basis of a Woods-Saxon distribution:

$$\frac{dN}{dr} = \frac{n_0}{1 + \mathrm{e}^{(r-R)/d}} \tag{13}$$

with parameters quoted in Ref. [19]:

$$n_0 = 0.17 \text{ fm}^{-3};\ R = 1.12A^{1/3} - 0.86A^{-1/3} \text{ fm};\ d = 0.54 \text{ fm}.$$

For each event, this Monte-Carlo calculation provides the number of nucleons $N_{1(a)}$ and $N_{1(b)}$ colliding once, in the projectile a and target nucleus b respectively. In general, these two numbers differ because nucleons from a may collide once with a nucleon from b, which in turn collides with two or more nucleons from a. Therefore, the minimum between $N_{1(a)}$ and $N_{1(b)}$ is the maximal number of single nucleon-nucleon collisions per event, i.e.

$$N_c \geq \min[N_{1(a)}, N_{1(b)}] \equiv N_m \tag{14}$$

The equality sign applies only if the N_m nucleons from one nucleus collided with N_m nucleons of the other, all of them among those undergoing one collision. We assume this is always the case and hence take N_m as a fair estimate of the number of single collisions. The mean number of N_c is then averaged over the most central bin defined by the distribution of the number of projectile spectators according to the NA49 centrality selection method.

We determined the mean number of single N-N collisions within the most central bin to be 2.67, 5.49 and 17.6 for C-C, Si-Si and Pb-Pb respectively at a beam energy of 158A GeV. By fixing N_c to the above numbers, we then fitted V, T and μ_B of the equilibrated fireballs and found the results shown in Table I. The fit quality is size-ably worse than in the previous case. Since the used number of collisions is actually an upper limit of single N-N collisions, we conclude that the SHM(TC) is disfavored by the data, if the Glauber model is assumed to be correct.

IV. ENERGY AND SYSTEM SIZE DEPENDENCE

We are now in a position to study the dependence of chemical freeze-out on beam energy and system size in central ultra relativistic heavy ion collisions. According to what has been discussed at the end of Sect. 2, for RHIC energy, we will include the parameters determined with fits to midrapidity particle multiplicity ratios.

The first observation is that the chemical freeze-out of different colliding systems at the same N-N centre-of-mass energy, i.e. C-C, Si-Si and Pb-Pb, seem to occur at similar values of the baryon chemical potential, namely $\mu_B \approx 250$ MeV (see Fig. 3). Such weak system size dependence of the baryon chemical potential has been already reported earlier [20]. On the other hand, systems with fewer participating nucleons seem to decouple at slightly higher temperature than heavy systems (see Fig. 3). Nevertheless, generally speaking, the freeze-out condition seems to be determined mostly by the beam energy and little by the number of participants, also in peripheral collisions [20, 21].

The dependence of the freeze-out parameters on the N-N centre-of-mass energy in heavier systems (Pb-Pb and Au-Au) is shown in Figs. 1,2. The fitted points show a relatively strong dependence on energy, yet with a smooth behaviour: lower energies always correspond to a lower central temperature value and a higher baryon chemical potential.

A smooth dependence is also obtained for the chemical freeze-out in the $\mu_B - T$ plane, see Fig. 7; all points lie, over the examined range of temperatures, on a parabola corresponding to chemical freeze-out condition $\langle E\rangle/\langle N\rangle \approx 1$ GeV [22]. Owing to the slight difference in temperature, the lighter systems C-C and Si-Si do not lie on the same curve and this leads to the conclusion that, at least in the model with γ_S only, freeze-out curve depends on colliding nucleus.

Conversely, the degree of chemical equilibration of strangeness seems to be strongly dependent on the number of participants, and much less on the energy. This has been pointed out in several studies of peripheral Pb-Pb collision systems [20, 21]. In fact, from small to large systems, γ_S increases monotonically from 0.45 in p-p to ~ 0.8 in Pb-Pb at the same beam energy, see Fig. 4, while the dependence on energy is much milder, with a variation from 0.65 to 0.84 over the 4.7-17.2 GeV energy range. Therefore, strangeness is not in chemical equilibrium up to SPS and only for midrapidity yields at RHIC γ_S seemed to have attained one [23].

Strong suppression in strangeness production in small systems can be seen also in the Wroblewski variable $\lambda_S = 2\langle s\bar{s}\rangle/(\langle u\bar{u}\rangle + \langle d\bar{d}\rangle)$, the estimated ratio of newly produced strange quarks to u, d quarks at primary hadron level, shown in Figs. 2,4, and Table I. The calculation of newly produced quark pairs is performed by using the statistical model best fit values of the various hadron multiplicities, so the obtained λ_S values are somehow model-dependent. Nevertheless, this variable shows a very similar behaviour as the γ_S parameter, indicating strong monotonic system size dependence in relative strangeness production.

It is also interesting to estimate the thermal energy content of the hadronic matter at freeze-out. Indeed, the fraction of thermal energy to the total available energy decreases rapidly as a function of energy, as shown in Fig. 5.

A. Interpolation of the statistical model parameters

It is worth trying to summarize the amount of information we have collected on the statistical model parameters at freeze-out in the central collisions of different systems with some simple empirical interpolations. Some of them have already been proposed in previous works [7, 24].

A satisfactory description of our Pb-Pb and Au-Au freeze-out points in the $T-\mu_B$ plane can be achieved by the simple parabolic fit:

$$T \approx T_0 - b\,\mu_B^2 \qquad T_0 = 167.5\,\mathrm{MeV} \quad b = 0.1583\,\mathrm{GeV}^{-2}. \tag{15}$$

Note that the most recent determination [25] of T and μ_B in central Au-Au collisions at $\sqrt{s}_{NN} = 130$ GeV (169±6 MeV and 38±5 MeV, respectively) also follows this dependence, see Fig. 7. Similarly, for γ_S, one can try to make an interpolation as a function of μ_B constrained by the requirement $\gamma_S \to 1$ when $\mu_B \to 0$, i.e. full chemical equilibrium at very large energy. The assumed functional form is then:

$$\gamma_S = 1 - g \exp\left[-\frac{a}{\mu_B/T}\right] \tag{16}$$

and the resulting parameters are $g = 0.396$ and $a = 1.23$. Both fits to Eqs. (15) and (16) have $\chi^2/dof \approx 1$.

The next step is to provide an interpolation of μ_B as a function of $\sqrt{s}_{NN}$. Once this was known, it would be possible to predict the value of T and γ_S at any collision energy through the Eqs. (15) and (16). The main advantage of μ_B is that it is almost independent of the number of participants, so that a single function $\mu_B = \mu_B(\sqrt{s}_{NN})$ would apply to both light and heavy systems. We have interpolated μ_B with a function:

$$\mu_B = \alpha \frac{\log \sqrt{s}_{NN}}{(\sqrt{s}_{NN})^{\beta}} \tag{17}$$

with $\alpha = 2.06$ and $\beta = 1.13$ and energy is given in GeV. This interpolation gives a very good description of the energy dependence of baryon chemical potential from $\sqrt{s}_{NN} = 4.7$ to 130 GeV.

We are now in a position to obtain the functions $T = T(\sqrt{s}_{NN}, A)$ and $\gamma_S = \gamma_S(\sqrt{s}_{NN}, A)$. According to Eqs. (15) and (17), we have:

$$T = T_0 - C\left(\frac{\log \sqrt{s}_{NN}}{(\sqrt{s}_{NN})^{\beta}}\right)^2 \tag{18}$$

where $C = b\alpha^2 \simeq 0.672$ and energy is given in GeV.

Furthermore, in order to take into account the dependence on the system size, we introduce a very simple A dependence for the constant T_0 term. Looking at Fig. 3 one can easily realize that T_0 depends almost logarithmically on the mass number of the nucleus, thus it can be assumed $T_0 = T_c - \tau \log A$ with $T_c \simeq 191.5$ MeV and $\tau \simeq 4.5$ MeV leading to the final expression of the chemical freeze-out temperature:

$$T = 0.1915 - 0.0045 \log A - 0.672\left(\frac{\log \sqrt{s}_{NN}}{(\sqrt{s}_{NN})^{1.13}}\right)^2 \tag{19}$$

where every quantity is expressed in GeV.

For γ_S, as its dependence on A is stronger than on $\sqrt{s}_{NN}$, it is more suitable to write down an independent interpolation formula rather than obtaining one from Eqs. (15), (16) and (17). By using

$$\gamma_S = 1 - \zeta \exp\left[-\xi\sqrt{A\sqrt{s}_{NN}}\right] \tag{20}$$

which is inspired of (17), a good fit is obtained by setting $\zeta = 0.606$ and $\xi = 0.0209$ (the energy is in GeV).

It should be emphasized that all of the above relations only apply to central collisions and cannot be used for peripheral nucleus-nucleus collisions. For instance, it has already been observed, indeed, that strangeness undersaturation does not scale with the number of participants [20], rather with the linear size of the fireballs [21].

V. DISCUSSION

In principle, by using equations (15)-(20), it is possible to estimate, within the SHM, the average multiplicities and ratios of any particle species for any colliding system in central collisions at any energy. It is especially interesting to study possible deviations of some specific particle ratios from the predicted smooth dependence of our interpolations. Such deviations would be a signal that the SHM scheme has some problem and either some refinement is needed (e.g. the hypotheses underlying the global fit do not fully apply) or there is some specific mechanism beyond the statistical ansatz responsible for them.

Of special importance in this context is the anomalous peak ("horn") in the ratio K^+/π^+ observed around beam energy 20A-30A GeV [6], which has been discussed in the statistical model in ref. [26]. Fig. 6 shows the experimental peak as a function of $\sqrt{s}_{NN}$ along with the statistical model prediction calculated by means of the interpolations (15)-(20) and taking $A = 208$ along the curve. The theoretical error band corresponds to the 1σ ($\simeq 68\%$) 7-dimensional ellipsoidal contour of the multivariate Gaussian distribution relevant to the 7 free parameters in our interpolating relations (15),(17),(20) (that is T_c, τ, b, α, β, ζ and ξ). In practice, this band has been determined through a Monte-Carlo procedure by randomly extracting 1000 times these parameters within the above contour and calculating, for each set, the K^+/π^+ ratio; the resulting minimum and maximum ratios were taken as the band bounds. The smooth interpolation of the SHM(γ_S) parameters fails to reproduce the horn because the model (see Table V) underestimates K^+ multiplicity at each energy point over the relevant range, especially at 20A and 30A GeV, where the discrepancy is of the order of 3 standard deviations. Pion multiplicities are also underestimated, but deviations are much less strong, especially at lower energies. In Fig.6, the corresponding $\langle K^- \rangle / \langle \pi^- \rangle$ ratio is shown as well. In Pb-Pb collisions, the statistical model tends to overestimate this ratio because K^- multiplicities are relatively well reproduced at all beam energies, but the π^- multiplicities are underestimated especially at the higher energies.

There are many possible reasons for this and other observed discrepancies, among them:

- a failure of the SHM(γ_S) scheme;
- an insufficient knowledge of the hadronic mass spectrum and branching ratios;
- an inadequacy of the assumptions needed to perform global fits, e.g. large fluctuations of charge distributions among the different clusters.

As far as the first item is concerned, we observe that the most straightforward way of overcoming these difficulties, is to add further parameters in the model, like the light-quark non-equilibrium parameter γ_q proposed in ref. [27]. However, unlike γ_S, the introduction of this new parameter does not imply a remarkable and systematic improvement in the statistical model fits for all collisions [28]. In fact, by making a careful scan of 4-parameters fit at 20A GeV, in the analysis A, we found that the best fit occurs at $\gamma_q = 0.7$, with $T \simeq 143$ MeV, $\mu_B/T \simeq 3.5$ with a $\chi^2/dof = 14.7/4$, i.e. only 0.8/4 units/dof less than the fit for $\gamma_q = 1$. On the other hand, at 30A GeV, we obtain a better fit ($\chi^2/dof = 9.5/4$ instead of 16.5/4) at $\gamma_q = 1.7$ with $T \simeq 124$ MeV and $\mu_B/T \simeq 3$, in agreement with ref. [9], at a price of an abrupt change of γ_q, of about 1 and of a decrease (contrary to the general trend) of temperature of 20 MeV within a range of only 1.4 GeV in centre-of-mass energy. Such rapid changes might be simply owing to random fluctuations generated by data overfitting and definitely need further investigations.

Concerning the second item, it should be emphasized that $\sim$70% of $\pi^\pm$ and $\sim$50% of K^- multiplicities originate from resonance decays, while for K^+ the contribution increases from 25% at AGS to $\sim$50% at RHIC. Although the uncertainty on the measured branching ratios do not play a significant role (see discussion in Sect. 3), the possible presence of many undetected resonances may affect the calculation of final yields. One of the most remarkable examples is the σ scalar resonance which is usually not included in these analyses. In fact, if the mass was 600 MeV and width 300 MeV, its inclusion would entail an enhancement of charged pion yield by about 20 units in Pb-Pb collisions at $\sqrt{s}_{NN} = 17.2$ GeV, which will make our fit better. However, it is difficult to conclude that the inclusion of this resonance would restore a perfect agreement with the data with still such a large uncertainty on its parameters.

Altogether, we deem that, among the above proposed explanations of the observed discrepancies, the third one is the most conservative. Non-statistical fluctuations of strangeness or baryon density, like those discussed e.g. in ref. [29], may invalidate the EGC assumption, thus affecting the global fit to particle multiplicities. Yet, this kind of alternative pictures still need to be probed with thorough comparison with the data.

The collisions between 20A and 40A GeV of beam energy are those showing the most significant discrepancies from the smooth SHM interpolations. This can be seen in Figs. 8, 9 and 10, where the correlations between different particle ratios are shown along with the predicted central values of the interpolations (15), (16) and (20) as smooth dashed lines. All of these ratios involve strangeness-carrying particles, which may suggest that a peculiar dynamical process involving strange quarks occurs around this energy region.

VI. SUMMARY AND CONCLUSIONS

We have analyzed the available hadronic multiplicities measured in central heavy ion collisions over an energy range $\sqrt{s}_{NN} = 4.5 - 17.2$ GeV within the statistical hadronization model. The thermal parameters of the source, baryon chemical potential and temperature, depend strongly on N-N centre-of-mass energy, but their behaviour is found to be smooth and we have been able to find empirical relations describing their dependence on energy up to the top RHIC energy. Conversely, at fixed energy, they depend little on the system size as we have found similar values for μ_B and T at chemical freeze-out for C-C, Si-Si and Pb-Pb.

On the other hand, chemical equilibration of strangeness is seen to be more dependent on the number of colliding nucleons than on energy, with the general trend for the strangeness under-saturation parameter γ_S to attain the value 1 only at energies $\sqrt{s}_{NN} = \mathcal{O}(100)$ GeV. Different versions of the SHM, aiming at explaining the observed under-saturation of the strange particle phase space, namely the two-component model described here and strangeness correlation volume model examined in ref. [7], seem to be disfavored by the data.

Discrepancies between the model with strangeness under-saturation parameter and the data have been pointed out with regard to specific particle ratios. The origin of these discrepancies, mostly in the beam energy region 20A-40A GeV, is still to be investigated.

Acknowledgments

This work was in partly supported by the NordForsk (J. M.) and Virtual Institute of Strongly Interacting Matter (VI-146) of Helmholtz Association, Germany.

References

[1] See e.g., U. W. Heinz, Nucl. Phys. A **661**, 140 (1999).
[2] F. Becattini, Z. Phys. C **69**, 485 (1996);
F. Becattini, U. Heinz, Z. Phys. C **76**, 269 (1997);
F. Becattini, G. Passaleva, Eur. Phys. J. C **23** 551 (2002);
F. Becattini, Nucl. Phys. A **702**, 336 (2002).
[3] R. Hagedorn, CERN lectures *Thermodynamics of strong interactions* (1970);
R. Hagedorn, CERN-TH 7190/94, in *Hot Hadronic Matter*, 13 (1994);
R. Stock, Phys. Lett. B **456**, 277 (1999).
[4] M. van Leeuwen et al., NA49 Coll., Nucl. Phys. **A715**, 161c (2003).
[5] M. Gazdzicki and M. I. Gorenstein, Acta Phys. Polon. B **30**, 2705 (1999).
[6] M. Gazdzicki *et al.*, NA49 Coll., J. Phys. G **30**, S701 (2004).
[7] F. Becattini, M. Gaždzicki, A. Keränen, J. Manninen and R. Stock, Phys. Rev. C **69** 024905 (2004).
[8] C. Alt *et al.* [NA49 Collaboration], Phys. Rev. Lett. **94**, 052301 (2005)
[9] J. Letessier and J. Rafelski, nucl-th/0504028.
[10] P. Braun-Munzinger, I. Heppe and J. Stachel, Phys. Lett. B **465**, 15 (1999).
[11] C. Blume, NA49 Collaboration, talk given at *Rencontres de Moriond*, hep-ph/0505137.
[12] I. G. Bearden *et al.*, BRAHMS Collaboration, Phys. Rev. Lett. **94**, 162301 (2005).
[13] I. G. Bearden *et al.*, BRAHMS Collaboration, Phys. Rev. Lett. **90**, 102301 (2003).
[14] S. Eidelman *et al.*, Phys. Lett. B **592**, 1 (2004).
[15] F. Becattini, G. Passaleva, Eur. Phys. J. C **23**, 551 (2002).
[16] F. Becattini, L. Ferroni, Eur. Phys. J. C **38**, 225 (2004).
[17] D. H. Rischke, M. I. Gorenstein, H. Stoecker and W. Greiner, Z. Phys. C **51**, 485 (1991).
[18] C. Hohne, F. Puhlhofer and R. Stock, arXiv:hep-ph/0507276.
[19] D. Miskoviec, http://www.linux.gsi.de∼misko/overlap.
[20] J. Cleymans, B. Kämpfer, P. Steinberg and S. Wheaton, hep-ph/0212335 (2002).
[21] F. Becattini, L. Maiani, F. Piccinini, A. D. Polosa and V. Riquer, hep-ph/0508188, to be published in Phys. Lett. B.
[22] J. Cleymans and K. Redlich, Phys. Rev. Lett. **81**, 5284 (1998).
[23] P. Braun-Munzinger, D. Magestro, K. Redlich and J. Stachel, Phys. Lett. B **518**, 41 (2001);
W. Florkowski, W. Broniowski and M. Michalec, Acta Phys. Polon. B **33**, 761 (2002).
[24] P. Braun-Munzinger, J. Cleymans, H. Oeschler and K. Redlich, Nucl. Phys. A **697**, 902 (2002).
[25] J. Cleymans, B. Kampfer, M. Kaneta, S. Wheaton and N. Xu, Phys. Rev. C **71**, 054901 (2005).
[26] J. Cleymans, H. Oeschler, K. Redlich and S. Wheaton, Phys. Lett. B **615**, 50 (2005).
[27] J. Letessier and J. Rafelski, Phys. Rev. C **59**, 947 (1999).
[28] F. Becattini, M. Gazdzicki and J. Sollfrank, Eur. Phys. J. C **5**, 143 (1998).
[29] V. Koch, A. Majumder and J. Randrup, nucl-th/0509030.
[30] S. V. Afanasev *et al.*, NA49 Coll., Phys. Lett. B **491**, 59 (2000);
J. Bachler *et al.*, NA49 Coll., Nucl. Phys. A **661**, 45 (1999);
D. Barna, NA49 Coll., Ph. D. Thesis, University of Budapest, (Hungary) 2004;
S. V. Afanasev *et al.*, NA49 Coll., J. Phys. G **27**, 367 (2001).
[31] I. Kraus [NA49 Collaboration], J. Phys. G **31**, S147 (2005)
[32] L. Ahle *et al.*, E-802 Coll., Phys. Rev. C **60** 044904 (1999).
[33] L. Ahle *et al.*, E-802 Coll., Phys. Rev. C **59** 2173 (1991).

[34] F. Becattini, J. Cleymans, A. Keränen, E. Suhonen, K. Redlich, Phys. Rev. C **64** 024901 (2001).
[35] L. Ahle *et al.*, E802 Coll., Phys. Rev. C **60** 064901 (1999).
[36] S. Ahmad *et al.*, Phys. Lett. B **382** 35 (1996).
[37] S. Albergo *et al.*, Phys. Rev. Lett. **88** 062301 (2002).
[38] C. Alt *et al.*, NA49 Coll., J. Phys. G **30**, S119 (2004).
[39] A. Richard [NA49 Collaboration], J. Phys. G **31**, S155 (2005).
[40] C. Blume [NA49 Collaboration], J. Phys. G **31**, S685 (2005)
[41] S. V. Afanasiev *et al.*, NA49 Coll., Phys. Lett. B **491**, 59 (2000); Phys. Lett. B **538** (2002) 275; Phys. Rev. C **66**, 054902 (2002).
[42] T. Anticic *et al.*, Phys. Rev. Lett. **93**, 022302 (2004).
[43] C. Meurer *et al.*, NA49 Coll., J. Phys. G **30**, S1325 (2004).
[44] C. Alt *et al.* [NA49 Collaboration], Phys. Rev. Lett. **94**, 192301 (2005)
[45] A. Mischke *et al.* Nucl. Phys. A **715**, 453 (2003).
[46] V. Friese *et al.*, NA49 Coll., Nucl. Phys. A **698**, 487 (2002).

TABLE III: Comparison between measured and fitted particle multiplicities, in the framework of SHM(γ_S) model, in p-p and central C-C (15.3% most central) and Si-Si (12.2%) collisions at a beam energy of 158A GeV.

	p-p 158A GeV (canonical)			C-C 158A GeV (S-canonical)			Si-Si 158A GeV (S-canonical)		
	Measurement	Fit A	Fit B	Measurement	Fit A	Fit B	Measurement	Fit A	Fit B
N_P				16.3 ± 1 [8]	15.79	15.98	41.4 ± 2 [8]	39.87	40.30
π^+	3.15±0.16 [30]	3.25	3.28	22.4 ± 1.6 [8]	22.3	22.0	56.6 ± 4.1 [8]	57.4	56.47
π^-	2.45±0.12 [30]	2.43	2.45	22.2 ± 1.6 [8]	22.3	22.0	57.6 ± 4.1 [8]	57.5	56.53
K^+	0.21±0.02 [30]	0.228	0.200	2.54 ± 0.25 [8]	2.71	2.79	7.44 ± 0.74 [8]	7.99	8.17
K^-	0.13±0.013 [30]	0.119	0.107	1.49 ± 0.16 [8]	1.46	1.51	4.42 ± 0.44 [8]	4.32	4.49
ϕ	0.012±0.0015 [30]	0.0203[a]	0.0149	0.18 ± 0.02 [8]	0.15	0.16	0.66 ± 0.09 [8]	0.48	0.51
Λ	0.115±0.012 [30]	0.133	0.117	1.32 ± 0.32 [8]	1.62	1.69	3.88 ± 0.58 [8]	4.57	4.87
$\bar{\Lambda}$	0.0148±0.0019 [30]	0.0147	0.0141	0.177 ± 0.028 [31]	0.149	0.182	0.492 ± 0.108 [31]	0.389	0.508
Ξ^-	0.0031±0.0003 [30]	0.00285	0.00110[a]		0.0728	0.0666		0.257	0.244
$\bar{\Xi}^+$	$9.2\,10^{-4} \pm 0.9\,10^{-5}$ [30]	0.000918	0.000388[a]		0.0151	0.0161		0.0485	0.0562
Ω	$2.6\,10^{-4} \pm 1.3\,10^{-4}$ [30]	$8.87\,10^{-5}$	$2.12\,10^{-5}$[a]		0.00397	0.00405		0.0181	0.0196
$\bar{\Omega}$	$1.6\,10^{-4} \pm 0.9\,10^{-4}$ [30]	$6.16\,10^{-5}$	$1.30\,10^{-5}$[a]		0.00179	0.00216		0.00736	0.00979
p		1.094	1.125		7.01	7.18		17.2	17.6
$\bar{p}$	0.040±0.007 [30]	0.0364	0.0445		0.303	0.367		0.714	0.879
K^0_S	0.18±0.04 [30]	0.14	0.15		2.05	2.14		6.06	6.37
π^0		3.32	3.10		25.0	23.2		64.3	59.7
η		0.382	0.279		2.64	2.09		6.78	5.59
ω		0.342	0.299		2.33	2.00		5.85	5.04
η'		0.0328	0.0165		0.210	0.132		0.537	0.374
ρ^+		0.449	0.467		2.75	2.84		6.92	7.11
ρ^-		0.301	0.305		2.75	2.85		6.94	7.16
ρ^0		0.408	0.428		2.84	2.94		7.14	7.39
K^{*+}		0.0878	0.0673		0.978	0.933		2.80	2.72
K^{*-}		0.0359	0.0275		0.462	0.437		1.35	1.29
K^{*0}		0.0741	0.0563		0.964	0.926		2.76	2.70
$\bar{K}^{*0}$		0.0405	0.0316		0.455	0.431		1.33	1.27
Δ^{++}		0.281	0.263		1.62	1.52		3.92	3.69
$\bar{\Delta}^{--}$		0.0063	0.00701		0.0686	0.0748		0.160	0.177
Σ^+		0.0413	0.0321		0.444	0.429		1.26	1.24
Σ^-		0.0276	0.0213		0.435	0.421		1.23	1.21
Σ^0		0.0358	0.0276		0.440	0.424		1.25	1.22
$\bar{\Sigma}^-$		0.00339	0.00295		0.0413	0.0472		0.111	0.131
$\bar{\Sigma}^+$		0.00445	0.00388		0.0403	0.0461		0.107	0.128
$\bar{\Sigma}^0$		0.00407	0.00352		0.0409	0.0466		0.109	0.130
Ξ^0		0.00323	0.00126		0.0740	0.0676		0.262	0.248
$\bar{\Xi}^0$		0.000849	0.000351		0.0152	0.0164		0.0494	0.0572
$\Lambda(1520)$	0.012±0.003 [30]	0.0106	0.00787		0.116	0.110		0.321	0.313
a - Excluded from the data sample in the fit									

TABLE IV: Comparison between measured and fitted particle multiplicities, in the framework of SHM(γ_S) model, in central Au-Au collisions (3%) at 11.6A GeV as well as Pb-Pb collisions (7%) at beam energies of 20A and 30A GeV.

	Au-Au 11.6A GeV (GC ensemble)			Pb-Pb 20A GeV (GC ensemble)			Pb-Pb 30A GeV (GC ensemble)		
	Measurement	Fit A	Fit B	Measurement	Fit A	Fit B	Measurement	Fit A	Fit B
N_P	363 ± 10 [32]	365.6	360.6	$349 \pm 1 \pm 5$ [6]	347.5	347.3	$349 \pm 1 \pm 5$ [38]	350.2	350.2
π^+	133.7 ± 9.93 [33, 34]	135.7	129.4	$184.5 \pm 0.6 \pm 13$ [6]	193.7	193.3	$239 \pm 0.7 \pm 17$ [38]	247.5	254.3
π^-		177.7	156.1	$217.5 \pm 0.6 \pm 15$ [6]	221.4	220.7	$275 \pm 0.7 \pm 19$ [38]	276.2	283.2
K^+	23.7 ± 2.86 [32]	18.7	18.8	$40.0 \pm 0.8 \pm 2.0$ [6]	34.4	35.7	$55.3 \pm 1.6 \pm 2.8$ [38]	44.8	43.9
K^-	3.76 ± 0.47 [32]	3.90	3.54	$10.4 \pm 0.12 \pm 0.5$ [6]	10.5	10.4	$16.1 \pm 0.2 \pm 0.8$ [38]	16.3	16.1
ϕ		0.327	0.350	1.91 ± 0.45 [6]	1.20	1.44	1.65 ± 0.17 [38]	2.01	2.08
Λ	18.1 ± 1.9 [7, 36, 37]	19.7	19.6	28.0 ± 1.5 [39]	28.8	31.2	$41.9 \pm 2.1 \pm 4.0$ [39]	33.8	34.5
$\bar{\Lambda}$	0.017 ± 0.005 [7, 36, 37]	0.017	0.011	0.16 ± 0.03 [40]	0.11	0.16	0.50 ± 0.04 [39]	0.35	0.49
p/π^+	1.23 ± 0.13 [34, 35]	1.27	1.22						
Ξ^-		0.551	0.557		1.37	1.42		1.85	1.66
$\bar{\Xi}^+$		0.00221	0.00244		0.0215	0.0340		0.0645	0.0846
Ω		0.0132	0.0147		0.0618	0.0758		0.105	0.104
$\bar{\Omega}$		0.000367	0.000571		0.00436	0.00936		0.0134	0.0204
p		172.5	155.1		143.6	142.0		142.0	142.6
$\bar{p}$		0.0302	0.0124		0.144	0.170		0.467	0.625
K^0_S		11.6	11.7		22.7	23.8		30.7	30.6
π^0		164.5	146.7		224.2	215.3		286.2	280.8
η		8.17	6.83		16.7	15.2		24.5	21.8
ω		5.03	3.62		11.3	9.50		17.8	15.9
η'		0.335	0.243		0.938	0.818		1.58	1.30
ρ^+		7.74	10.3		15.2	18.5		22.5	26.7
ρ^-		9.19	12.6		17.5	21.5		25.5	30.4
ρ^0		8.56	11.5		16.6	20.4		24.6	29.2
K^{*+}		3.59	3.50		8.38	8.93		12.4	12.2
K^{*-}		0.627	0.513		2.19	2.07		3.93	3.67
K^{*0}		3.80	3.81		8.75	9.50		12.9	12.8
$\bar{K}^{*0}$		0.564	0.459		2.01	1.89		3.65	3.41
Δ^{++}		25.6	24.2		26.5	25.4		27.9	26.8
$\bar{\Delta}^{--}$		0.00330	0.00222		0.0296	0.0332		0.100	0.126
Σ^+		4.81	4.75		7.54	7.65		8.92	8.46
Σ^-		5.43	5.48		8.30	8.49		9.67	9.21
Σ^0		5.13	5.10		7.94	8.05		9.32	8.82
$\bar{\Sigma}^-$		0.00363	0.00323		0.0329	0.0449		0.103	0.136
$\bar{\Sigma}^+$		0.00295	0.00257		0.0278	0.0379		0.0889	0.118
$\bar{\Sigma}^0$		0.00328	0.00288		0.0303	0.0412		0.0959	0.127
Ξ^0		0.537	0.535		1.34	1.39		1.83	1.62
$\bar{\Xi}^0$		0.00248	0.00270		0.0231	0.0366		0.0686	0.0899
$\Lambda(1520)$		0.776	0.777		1.47	1.58		1.94	1.91

TABLE V: Comparison between measured and fitted particle multiplicities, in the framework of SHM(γ_S) model, in central Pb-Pb collisions at beam energies of 40 and 80 (7% most central) and 158A GeV (5% most central). The measured $\Lambda(1520)$ yield has been removed from the fitted data sample at 158A GeV.

	Pb-Pb 40A GeV (GC ensemble)			Pb-Pb 80A GeV (GC ensemble)			Pb-Pb 158A GeV (GC ensemble)		
	Measurement	Fit A	Fit B	Measurement	Fit A	Fit B	Measurement	Fit A	Fit B
N_P	$349 \pm 1 \pm 5$ [41]	351.4	351.2	$349 \pm 1 \pm 5$ [41]	351.2	351.0	$362 \pm 1 \pm 5$ [41]	363.2	363.4
π^+	$293 \pm 3 \pm 15$ [41]	283.4	285.1	$446 \pm 5 \pm 22$ [41]	420.1	419.4	$619 \pm 17 \pm 31$ [41]	550.0	533.6
π^-	$322 \pm 3 \pm 16$ [41]	312.6	314.6	$474 \pm 5 \pm 23$ [41]	450.6	450.4	$639 \pm 17 \pm 31$ [41]	582.0	565.9
K^+	$59.1 \pm 1.9 \pm 3$ [41]	52.1	52.1	$76.9 \pm 2 \pm 4$ [41]	71.6	71.0	$103 \pm 5 \pm 5$ [41]	103.1	103.6
K^-	$19.2 \pm 0.5 \pm 1.0$ [41]	20.8	20.8	$32.4 \pm 0.6 \pm 1.6$ [41]	36.5	36.4	$51.9 \pm 1.9 \pm 3$ [41]	59.3	59.3
ϕ	2.50 ± 0.25 [6]	2.70	2.77	4.58 ± 0.20 [6]	4.43	4.46	7.6 ± 1.1 [41]	8.01	8.59
Λ	$43.0 \pm 1.9 \pm 3.4$ [42]	37.1	38.2	$44.7 \pm 2.8 \pm 3.2$ [42]	42.4	43.2	$44.9 \pm 3.5 \pm 5.4$ [42]	53.6	55.9
$\bar{\Lambda}$	$0.66 \pm 0.04 \pm 0.06$ [42]	0.67	0.64	$2.02 \pm 0.25 \pm 0.20$ [42]	2.16	2.11	$3.74 \pm 0.19 \pm 0.43$ [42]	4.83	4.96
Ξ^-	$2.41 \pm 0.15 \pm 0.24$ [43]	2.20	2.10		2.83	2.62	4.45 ± 0.22 [41]	4.42	4.31
$\bar{\Xi}^+$		0.122	0.112		0.330	0.298	0.83 ± 0.04 [41]	0.79	0.78
Ω		0.143	0.148		0.222	0.221	$0.59 \pm 0.12 \pm 0.04$ [44]	0.44	0.49
$\bar{\Omega}$		0.0262	0.0268		0.0623	0.0610	$0.26 \pm 0.06 \pm 0.03$ [44]	0.16	0.19
$\Omega + \bar{\Omega}$	$0.14 \pm 0.03 \pm 0.04$ [44]	0.17	0.18						
p		140.8	140.7		140.8	141.3		143.4	142.8
$\bar{p}$		0.897	0.821		3.32	3.21		6.86	6.70
K^0_S		36.4	37.1		53.5	54.4	81 ± 4 [45]	80.0	82.6
π^0		328.1	314.1		485.0	458.1		636.2	581.6
η		30.2	26.1		49.5	41.6		70.5	62.2
ω		22.7	18.5		39.9	33.0		55.4	44.7
η'		2.11	1.60		3.76	2.75		5.73	4.41
ρ^+		27.9	29.7		46.7	47.2		63.4	60.9
ρ^-		31.3	33.5		50.9	51.8		68.2	66.1
ρ^0		30.3	32.5		50.2	51.1		68.0	66.1
K^{*+}		15.6	14.3		23.0	20.9		34.2	31.8
K^{*-}		5.41	4.80		10.6	9.46		18.0	16.2
K^{*0}		15.6	14.9		23.5	21.6		34.7	32.5
$\bar{K}^{*0}$		5.06	4.47		10.0	8.95		17.2	15.5
Δ^{++}		28.7	26.4		29.9	27.5		30.9	28.1
$\bar{\Delta}^{--}$		0.198	0.163		0.747	0.650		1.55	1.36
Σ^+		9.79	9.47		11.3	10.8		14.4	14.0
Σ^-		10.5	10.2		11.9	11.4		15.0	14.6
Σ^0		10.2	9.83		11.6	11.1		14.7	14.3
$\bar{\Sigma}^-$		0.197	0.179		0.623	0.577		1.38	1.34
$\bar{\Sigma}^+$		0.172	0.157		0.561	0.520		1.26	1.23
$\bar{\Sigma}^0$		0.185	0.167		0.592	0.547		1.32	1.28
Ξ^0		2.17	2.07		2.81	2.60		4.41	4.29
$\bar{\Xi}^0$		0.129	0.119		0.345	0.312		0.823	0.812
$\Lambda(1520)$		2.27	2.09		2.78	2.53	1.57 ± 0.44 [46]	3.64	3.41

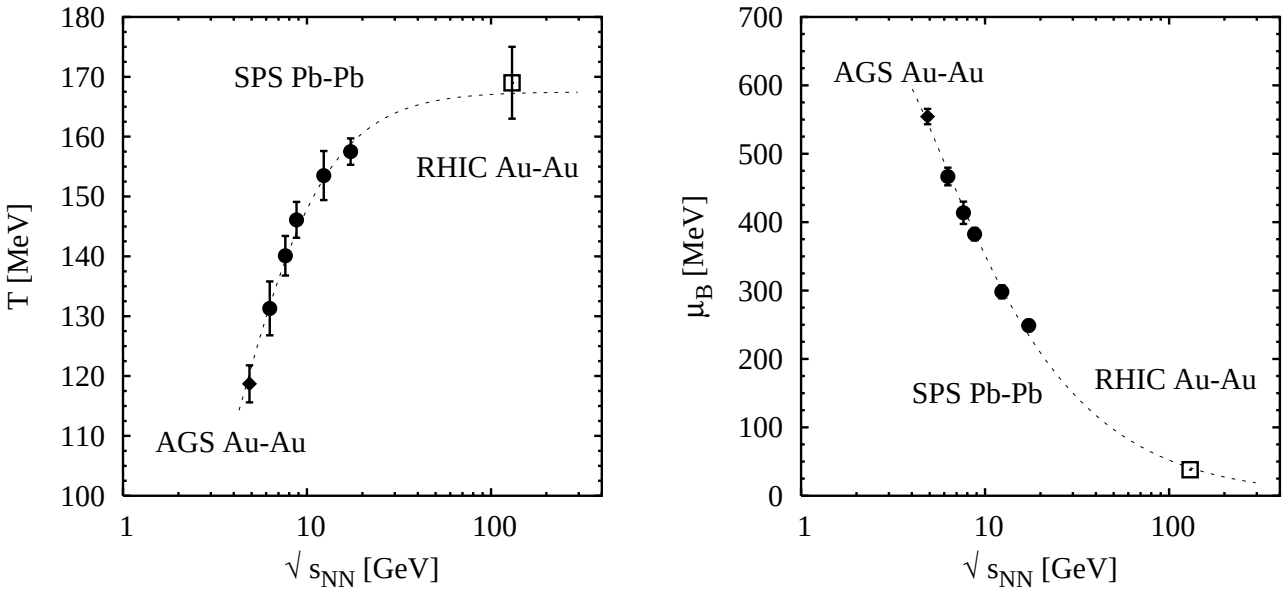

FIG. 1: LEFT: Fitted temperature at chemical freeze-out (analysis A) as a function of the N-N centre-of-mass energy in central Pb-Pb and Au-Au collisions. The dashed line is evaluated with the Eqs. (15) and (17). The RHIC point, obtained with a fit to hadron ratios at midrapidity [25] is shown as an open square.
RIGHT: Fitted baryon chemical potential at chemical freeze-out (analysis A) as a function of the N-N centre-of-mass energy in central heavy ion collisions. The dashed line is evaluated with the Eq. (17). The RHIC point, obtained with a fit to hadron ratios at midrapidity [25] is shown as an open square.

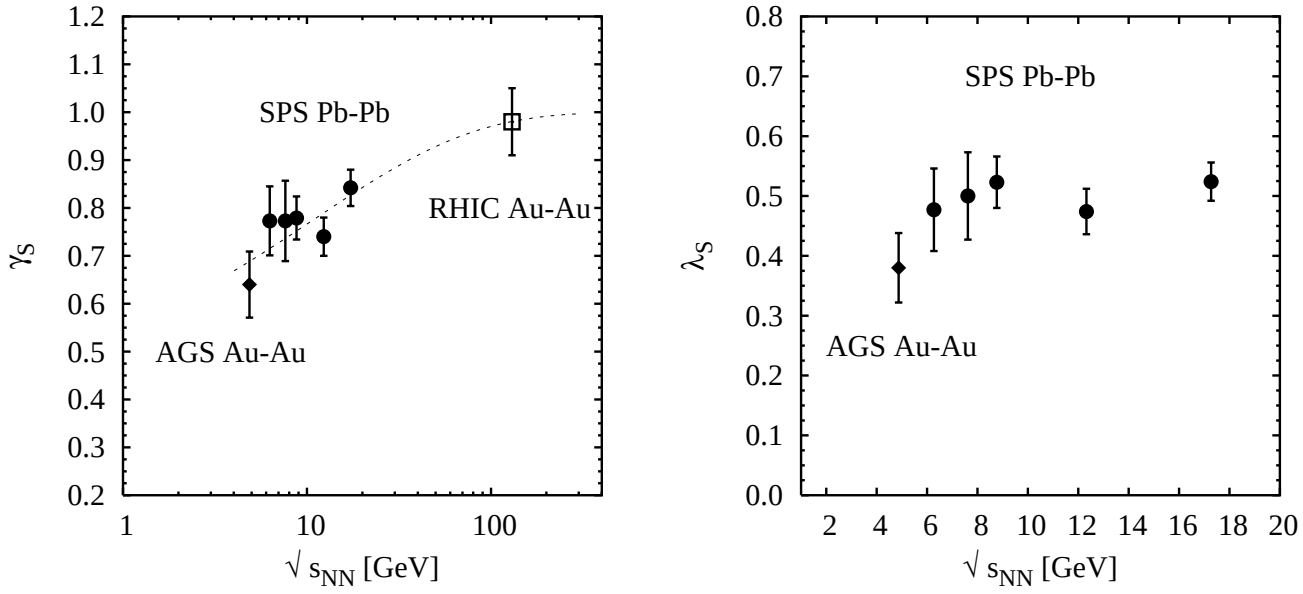

FIG. 2: LEFT: Strangeness undersaturation parameter γ_S at chemical freeze-out (analysis A) as a function of N-N centre-of-mass energy in central heavy ion collisions. The dashed line is evaluated with the Eq. (20). The RHIC point, obtained with a fit to hadron ratios at midrapidity [25] is shown as a square dot.
RIGHT: The Wroblewski factor λ_S (analysis A).

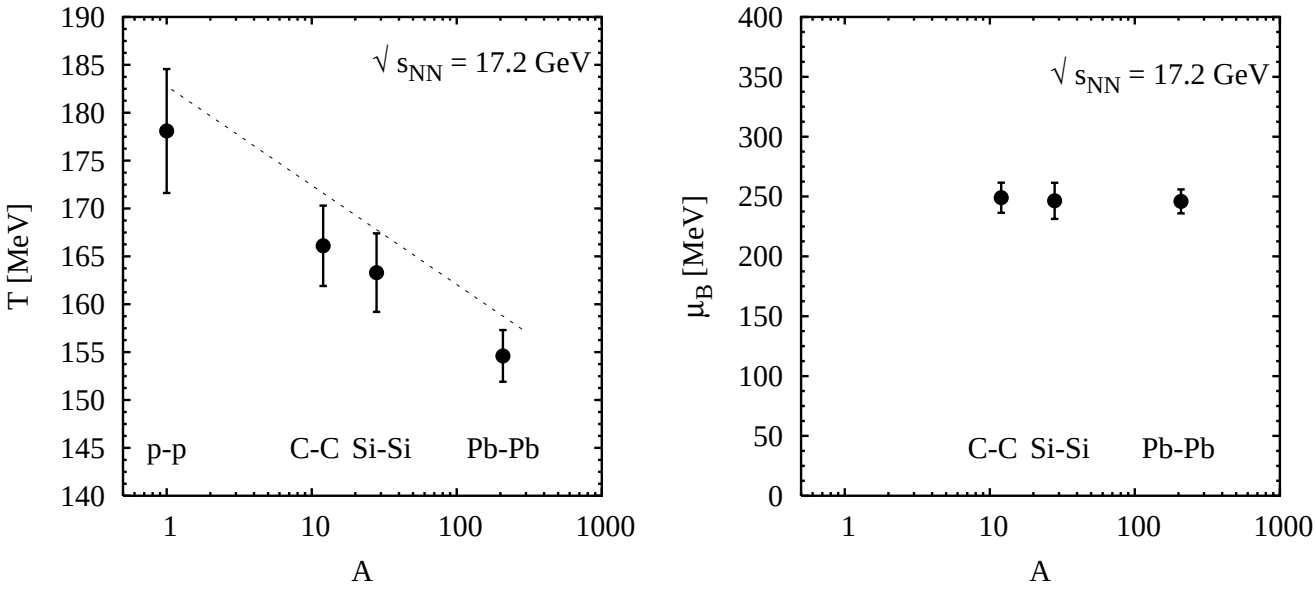

FIG. 3: Fitted temperature (LEFT) and baryon chemical potential (RIGHT) at chemical freeze-out as a function of A in central heavy ion collisions at $\sqrt{s}_{NN} = 17.2$ GeV. From left to right: p-p, C-C, Si-Si and Pb-Pb points fitted in analysis B. The dashed line is evaluated with the Eq. (19) which has been fitted to the points of analysis A. The observed systematic shift between data and interpolation is mainly a reflection of the slight difference ($\simeq 3-4$ MeV) between temperature in analyses A and B in Pb-Pb and p-p.

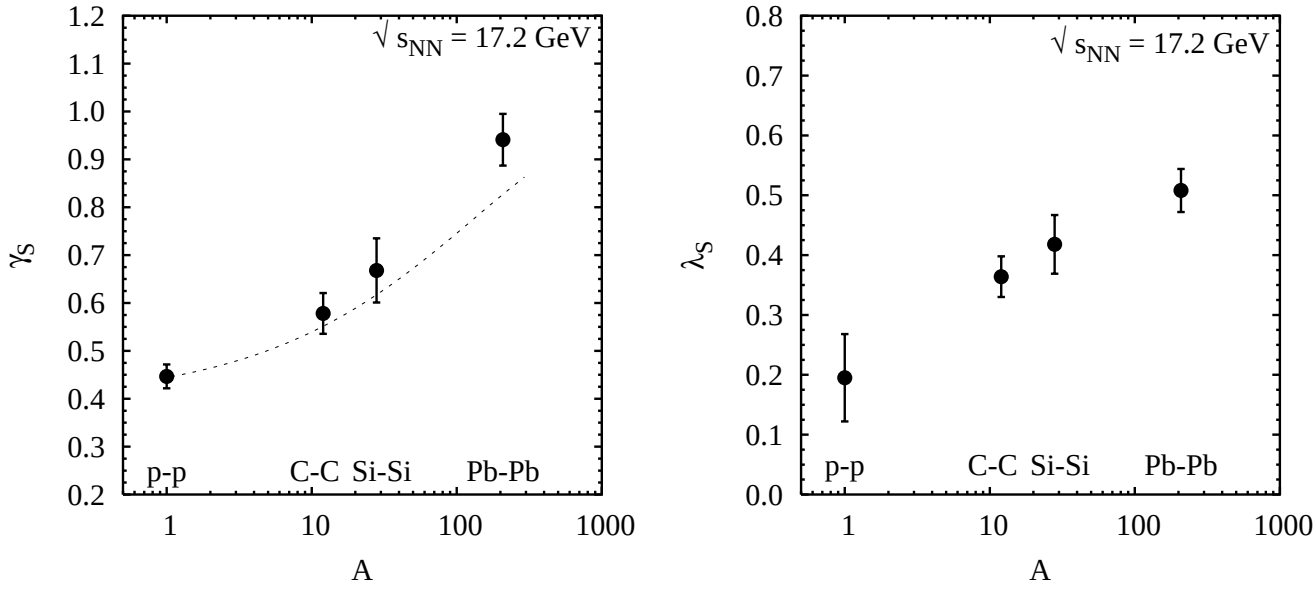

FIG. 4: Strangeness suppression factor γ_S (LEFT) and the Wroblewski factor λ_S (RIGHT) at chemical freeze-out as a function of A in central heavy ion collisions at $\sqrt{s}_{NN} = 17.2$ GeV (analysis B). From left to right: p-p, C-C, Si-Si and Pb-Pb. The dashed line is evaluated with the Eq. (20).

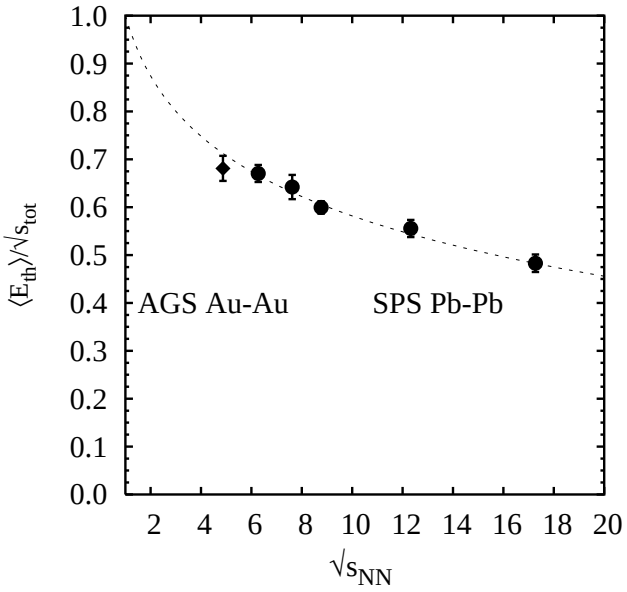

FIG. 5: Estimated fraction of the initial collision energy spent into thermal energy content in central heavy ion collisions as a function of the N-N centre-of-mass energy. The line is of the form $f(\sqrt{s}_{NN}) = 1 - b\ln(\sqrt{s}_{NN})$ and fitted to all points.

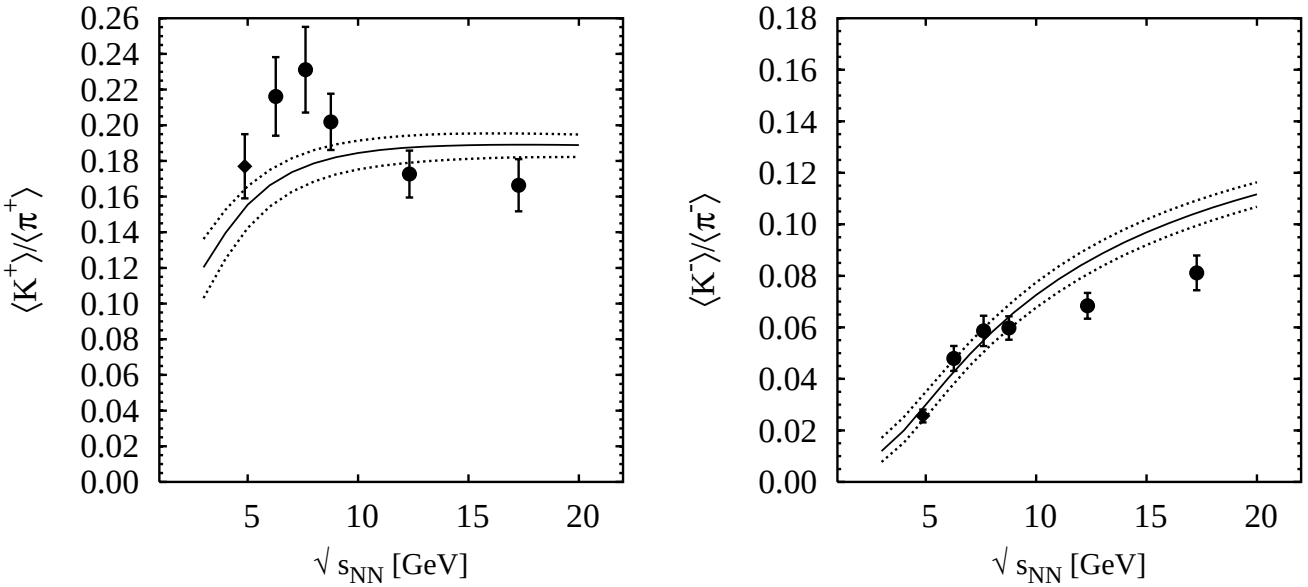

FIG. 6: Experimental vs interpolated $\langle K^+\rangle/\langle\pi^+\rangle$ -ratios (LEFT) and $\langle K^-\rangle/\langle\pi^-\rangle$ -ratios (RIGHT) in central heavy ion collisions as a function of $\sqrt{s}_{NN}$. The "horn" structure around $\sqrt{s}_{NN} \sim 7-8$ GeV is clearly visible. The bands have been calculated by using statistical model interpolating equations (15), (17),(20) with their central best fit parameters and errors (see text).

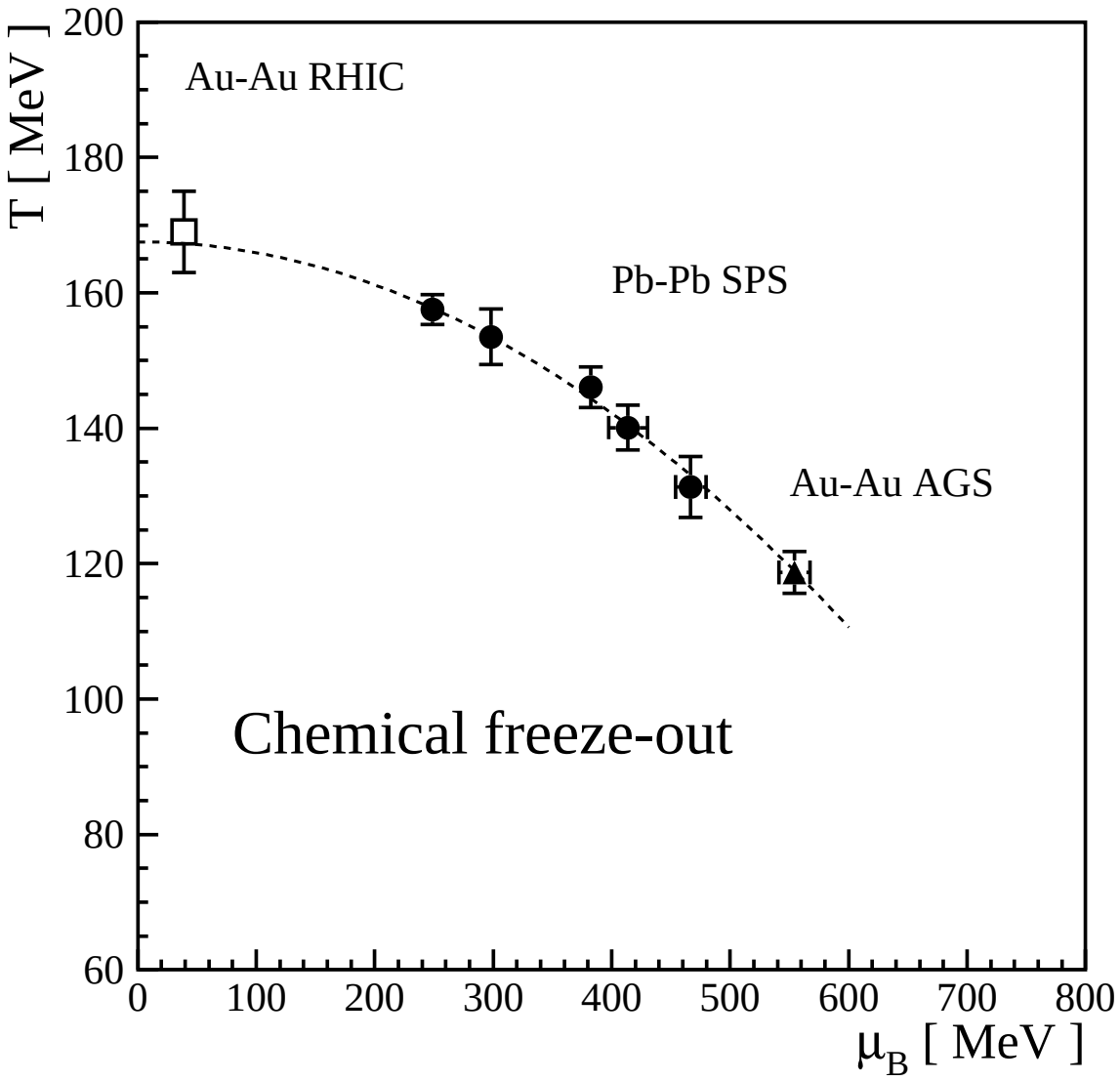

FIG. 7: Chemical freeze-out points in the $\mu_B - T$ plane for central Pb-Pb and Au-Au collisions. The dashed line shows the parabolic interpolation Eq. (15) obtained by fitting SPS and AGS points. The RHIC $\sqrt{s}_{NN} = 130$ GeV point, shown as an open square, has been taken from the recent analysis in ref. [25].

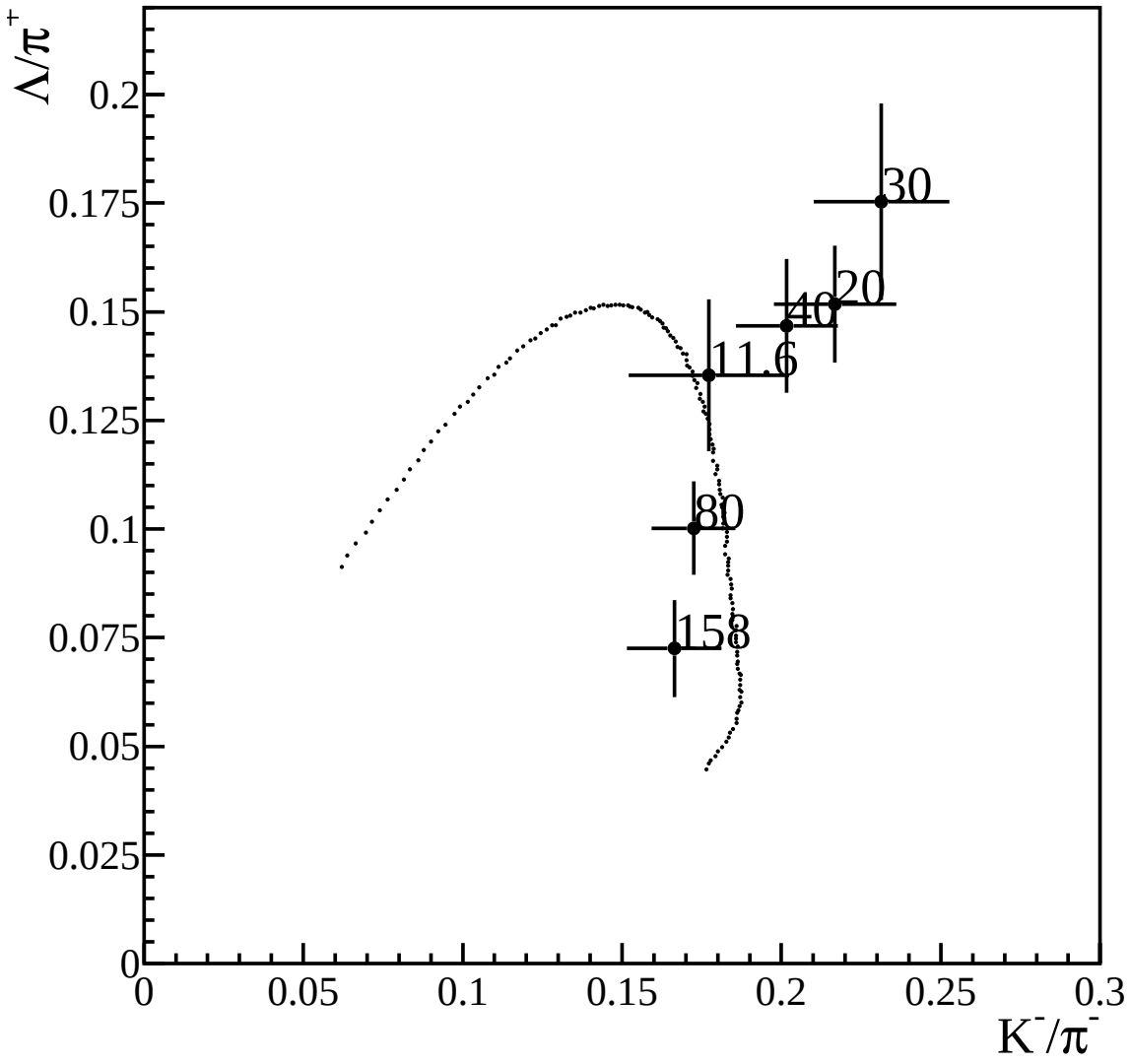

FIG. 8: The Λ/π^+ vs K^-/π^- ratios measured in Pb-Pb and Au-Au collisions at various beam energies. The dashed line shows the central predicted values of the interpolations (15) and (16) with their best fit parameters.

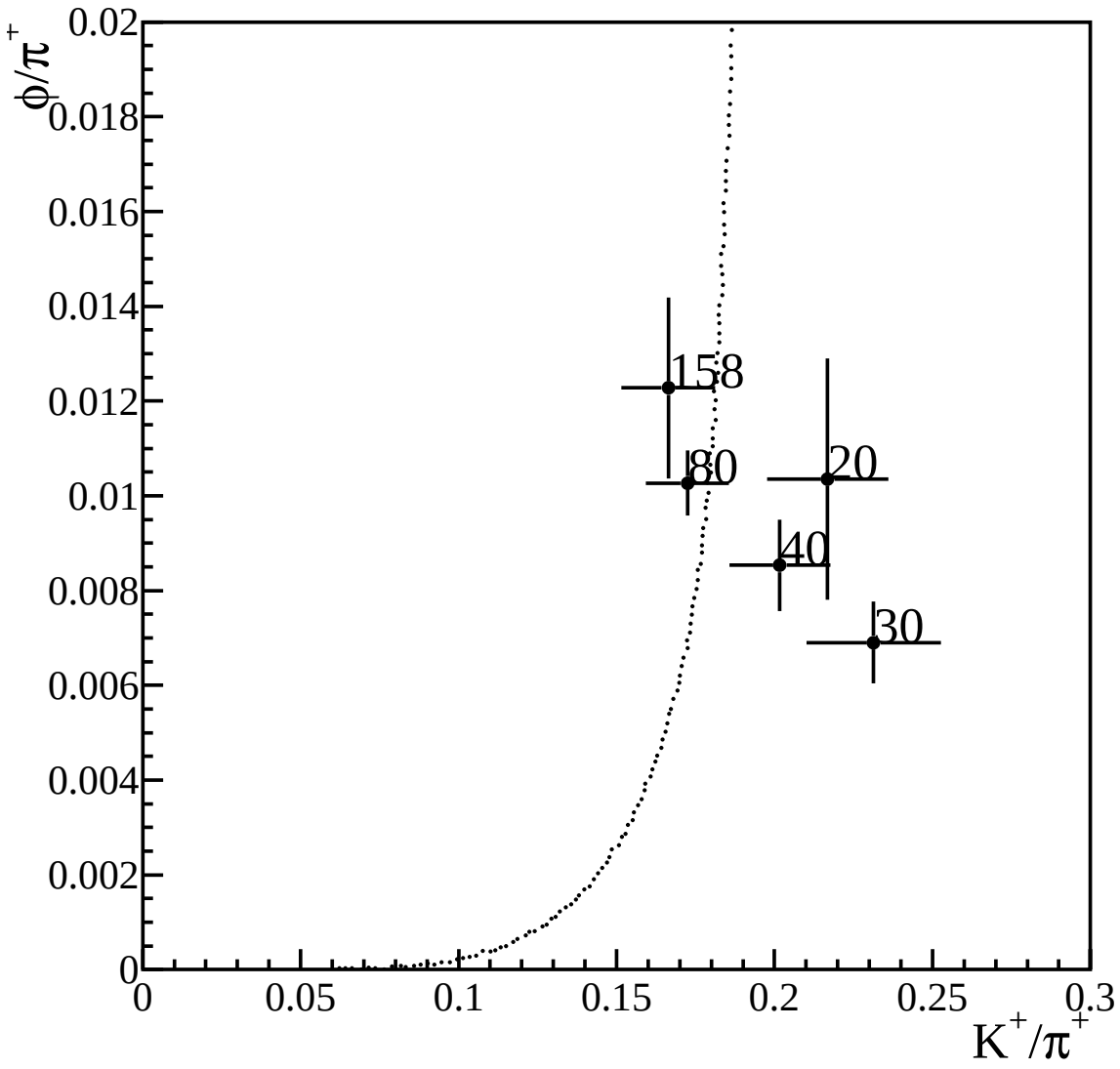

FIG. 9: The ϕ/π^+ vs K^+/π^+ ratios measured in Pb-Pb and Au-Au collisions at various beam energies. The dashed line shows the central predicted values of the interpolations (15) and (16) with their best fit parameters.

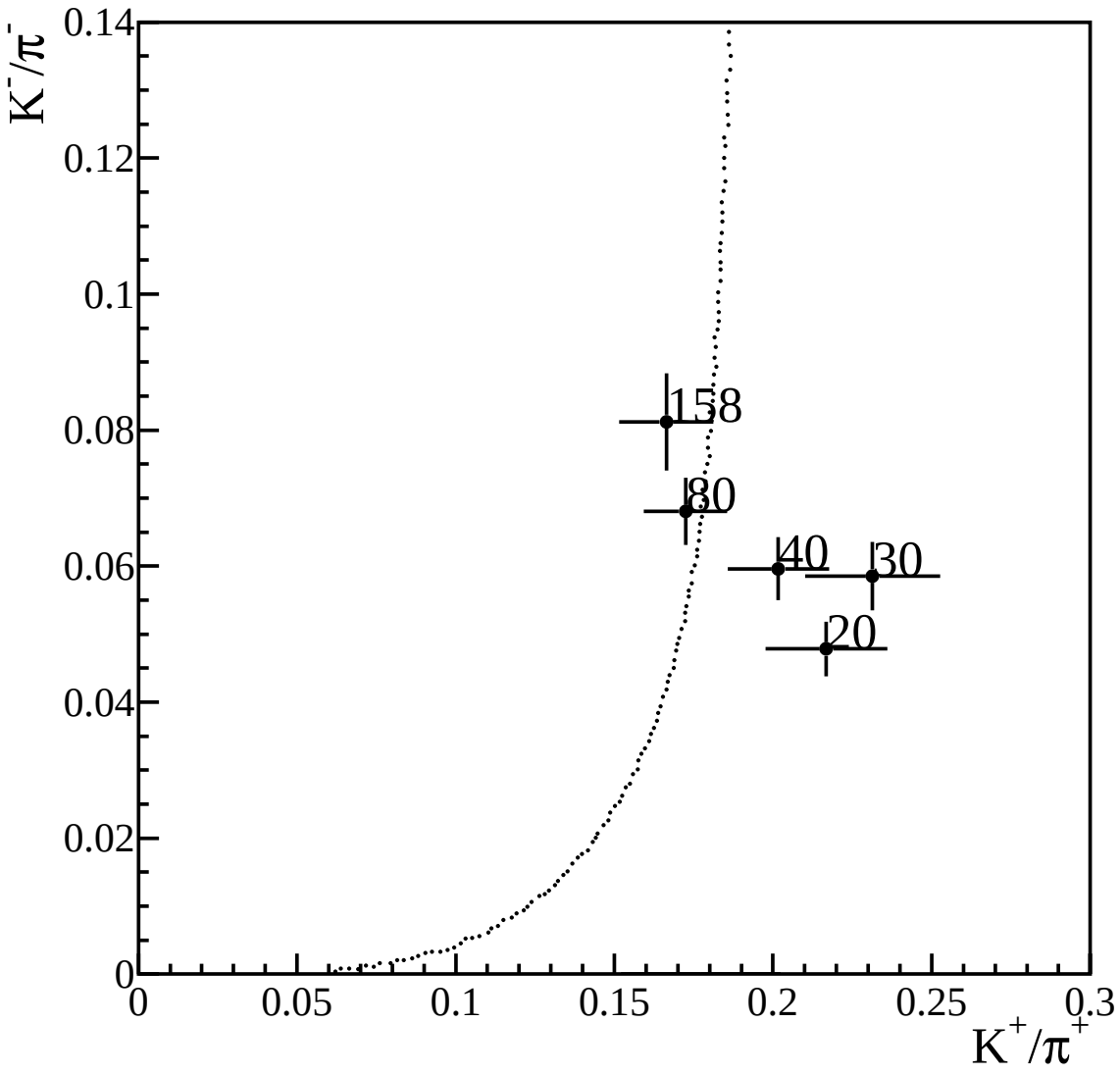

FIG. 10: The K^+/π^+ vs K^-/π^- ratios measured in Pb-Pb and Au-Au collisions at various beam energies. The dashed line shows the central predicted values of the interpolations (15) and (16) with their best fit parameters.